PLOS BIOLOGY

DISCOVERY REPORT

Carbon dioxide regulates cholesterol levels through SREBP2

Nityanand Bolshette[1], Saar Ezagouri[1], Vaishnavi Dandavate[1], Iuliia Karavaeva[1], Marina Golik[1], Hu Wang[2], Peter J. Espenshade[3], Timothy F. Osborne[4], Xianlin Han[2], Gad Asher[1]*

1 Department of Biomolecular Sciences, Weizmann Institute of Science, Rehovot, Israel, **2** The Sam & Ann Barshop Institute for Longevity & Aging Studies, University of Texas Health Science Center, San Antonio, Texas, United States of America, **3** Department of Cell Biology, Johns Hopkins University School of Medicine, Baltimore, Maryland, United States of America, **4** Institute for Fundamental Biomedical Research, Johns Hopkins All Children's Hospital, and Medicine in the Division of Endocrinology, Diabetes and Metabolism of the Johns Hopkins University School of Medicine, Petersburg, Florida, United States of America

* gad.asher@weizmann.ac.il

The Editors encourage authors to publish research updates to this article type. Please follow the link in the citation below to view any related articles.

Citation: Bolshette N, Ezagouri S, Dandavate V, Karavaeva I, Golik M, Wang H, et al. (2023) Carbon dioxide regulates cholesterol levels through SREBP2. PLoS Biol 21(11): e3002367. https://doi.org/10.1371/journal.pbio.3002367

Academic Editor: Giovanni D'Angelo, Ecole polytechnique federale de Lausanne Faculte des sciences de la vie, SWITZERLAND

Received: April 19, 2023

Accepted: October 6, 2023

Published: November 15, 2023

Data Availability Statement: GEO database (accession number GSE196294).

Funding: G.A. is supported by the Abisch Frenkel Foundation for the Promotion of Life Sciences, Adelis Foundation, Susan and Michael Stern, Yotam project and the Weizmann institute sustainability and energy research initiative. I.K. received the Novo Nordisk Foundation postdoctoral

Abstract

In mammals, O_2 and CO_2 levels are tightly regulated and are altered under various pathological conditions. While the molecular mechanisms that participate in O_2 sensing are well characterized, little is known regarding the signaling pathways that participate in CO_2 signaling and adaptation. Here, we show that CO_2 levels control a distinct cellular transcriptional response that differs from mere pH changes. Unexpectedly, we discovered that CO_2 regulates the expression of cholesterogenic genes in a SREBP2-dependent manner and modulates cellular cholesterol accumulation. Molecular dissection of the underlying mechanism suggests that CO_2 triggers SREBP2 activation through changes in endoplasmic reticulum (ER) membrane cholesterol levels. Collectively, we propose that SREBP2 participates in CO_2 signaling and that cellular cholesterol levels can be modulated by CO_2 through SREBP2.

Introduction

A fundamental process in mammalian physiology is oxygen (O_2) uptake from the environment into cells in exchange of carbon dioxide (CO_2), a byproduct of energy generation upon aerobic respiration. Oxygen is an essential substrate for cellular metabolism and bioenergetics and is indispensable for normal physiology and survival. Consequently, mammals have developed mechanisms to sense O_2 levels and regulate O_2 consumption in order to cope with conditions of insufficient O_2 supply. A principal regulator in the response to low oxygen levels is the hypoxia-inducible factor (HIF), which participates in sensing of low oxygen levels and subsequently activates a transcriptional program that facilitates cellular adaptation to changes in oxygen levels [1–3]. While the cellular response to oxygen levels is well characterized, relatively little is known regarding the mechanisms that participate in response to changes in CO_2 levels. It is noteworthy that CO_2 plays various critical roles in mammalian physiology including regulation of blood pH, respiratory drive, and O_2 affinity for hemoglobin [4]. Under physiological conditions, arterial blood CO_2 levels are tightly maintained approximately 35 to 45 mm Hg

fellowship. P.J.E. and T.F.O. are supported by grants from the National Institute of Health (HL077588 and GM149312 to P.J.E. and DK124343 to T.F.O.). The funders had no role in study design, data collection and analysis, decision to publish, or preparation of the manuscript.

Competing interests: The authors have declared that no competing interests exist.

Abbreviations: COPD, chronic obstructive pulmonary disease; ER, endoplasmic reticulum; HIF, hypoxia-inducible factor; INSIG, insulin-induced gene; MBCD, methyl-beta-cyclodextrin; OSA, obstructive sleep apnea; PCA, principal component analysis; SCAP, SREBP cleavage-activating protein; SRE, sterol regulatory element; TTF, tail tip fibroblast; UMI, unique molecular identifier.

(approximately 5%). Altered CO_2 levels are associated with the pathophysiology of various diseases such as chronic obstructive pulmonary disease (COPD) and obstructive sleep apnea (OSA) as well as impaired wound healing and fibrosis [5–7].

Carbon dioxide molecules are transported in the blood from body tissues to the lungs by one of 3 methods: dissolution directly into the blood, binding to hemoglobin, or carried as a bicarbonate ion. About 10% of CO_2 is dissolved in the plasma, a small fraction is bound to hemoglobin, while the majority (about 85%) is carried as a part of the bicarbonate buffer system [4]. In aqueous solution, CO_2 reacts with the water to form carbonic acid (H_2CO_3), which is readily buffered by the bicarbonate buffer system to maintain the pH levels within the physiological range [8].

To identify signaling pathways that regulate gene expression in response to changes in CO_2 levels, and hence participate in CO_2 sensing, we employed a cell culture setup alongside high-throughput transcriptomic and biochemical analyses. We found that CO_2 activates a distinct transcriptional response that is dependent on SREBP2, a key regulator of cholesterol biosynthesis, to regulate the expression of cholesterogenic genes and cholesterol accumulation. SREBP2 regulation by CO_2 is likely mediated by changes in endoplasmic reticulum (ER) membrane cholesterol levels. We, thus, propose that SREBP2 plays a role in cellular CO_2 signaling and that SREBP2 regulation of cholesterol levels can be modulated by changes in CO_2 levels.

Results

The transcriptional response to low CO_2 differs from pH

To identify signaling pathways that participate specifically in CO_2 sensing and not changes in pH, we examined the global transcriptional response of cultured cells to reduction in CO_2 levels from 5% to 1%. We used special chambers with CO_2, O_2 and temperature controls [9]. Temperature, O_2 and CO_2, levels were continuously monitored throughout the experiment with constant temperature of 37˚C and 20% O_2. While CO_2 levels were modulated by replacing them with the inert nitrogen gas and were kept either at 5% or 1% (Fig 1A).

As aforementioned, once CO_2 reacts with aqueous solution it forms carbonic acid and acidifies it. Since the reduction in CO_2 levels from 5% to 1% resulted in alkaline condition, we also used 18 mM NaOH to alkalize the media as a control for changes that are purely pH-dependent. Importantly, under both conditions, namely 1% CO_2 or 18 mM NaOH, the media pH at 2 and 4 h post exposure was similar (approximately 7.7) and differed from that of control cells (5% CO_2), which maintained pH across the normal physiological range (approximately 7.3) (Fig 1B). NIH3T3 cells (a fibroblast cell line that was isolated from mouse NIH/Swiss embryos) were harvested 2 and 4 h post exposure, RNA was extracted and analyzed by RNA-sequencing. The transcriptomic analysis revealed that the transcriptional response differed between the low CO_2 exposure and the alkaline conditions, even though the pH was similar (Figs 1C and 1D and S1). Notably, principal component analysis (PCA) and unsupervised clustering analyses (Fig 1C and 1D) clearly discriminated between exposure to low CO_2 versus NaOH treatment. NaOH treatment induced a prominent effect on gene expression with 2,697 genes showing differential response (P adj. $<= 0.05$, $|\log2FC| >= 1$, baseMean $>= 5$), with 1,320 up- and 1,377 down-regulated. While exposure to a low CO_2 level led to a milder effect on gene expression (1,328 genes with 685 up- and 643 down-regulated) (S1A and S1B Fig). Although, both the up- and down-regulated genes overlapped between the CO_2 and NaOH groups, we found in line with the PCA and cluster analyses that a significant number of genes are uniquely altered in response to CO_2 (S1B Fig).

Overall, our analyses show that under similar alkaline pH, the transcriptional response differs between low CO_2 and NaOH treatments. Thus, supporting a distinct mechanism that is activated in response to changes in CO_2 levels to regulate gene expression.

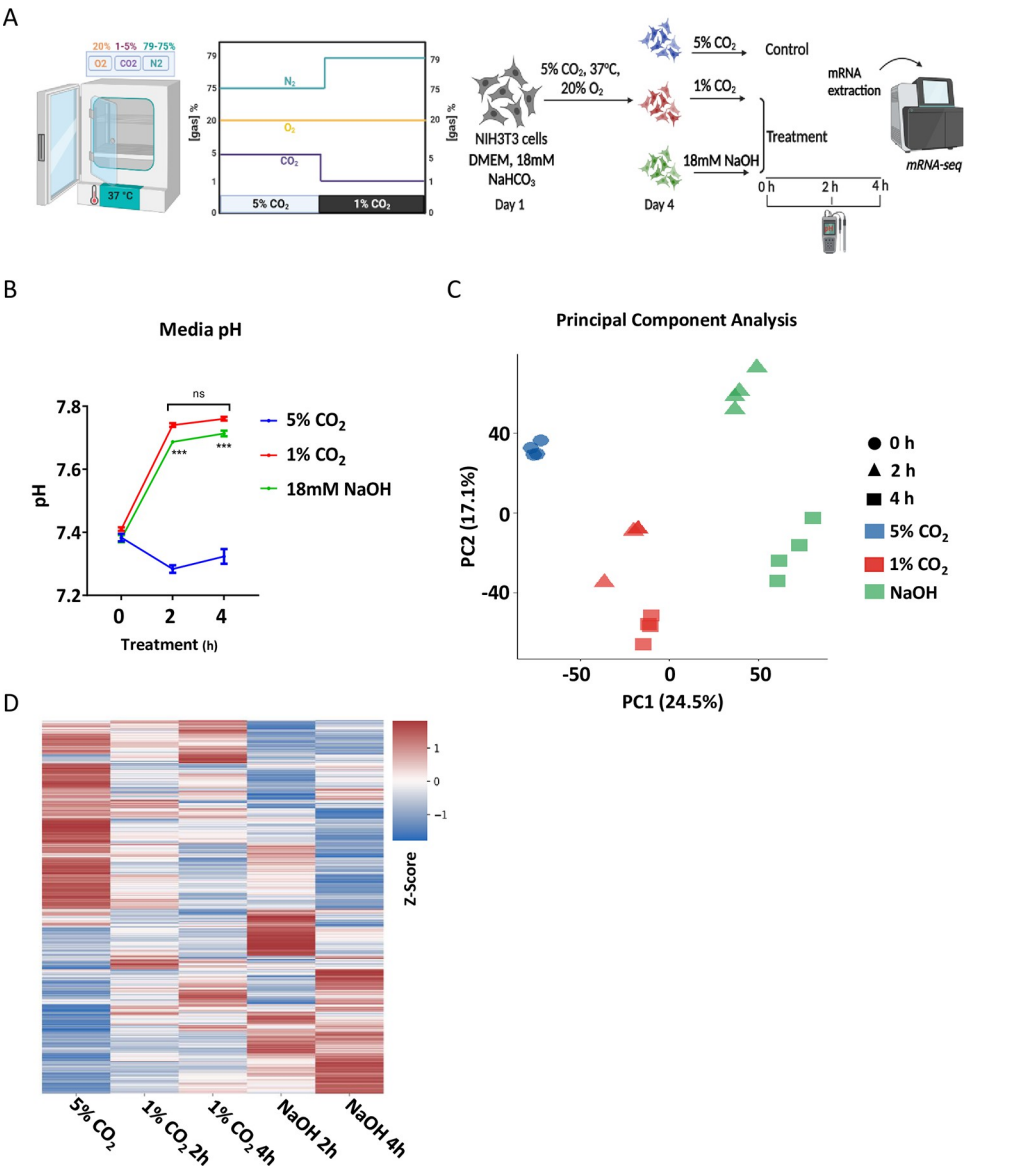

Fig 1. The transcriptional response to low CO_2 levels compared to NaOH treatment. (**A**) A schematic depiction of the experimental design. NIH3T3 cells were cultured in media B (as detailed in method) at 37˚C with 5% CO_2 and 20% oxygen. On day 4, cells were either untreated or treated with 18 mM NaOH or shifted to a special incubator (Coy Labs, USA) with 1% CO_2 and 20% oxygen. Cells and media were collected 2 and 4 h post treatment. RNA was extracted and analyzed by RNA sequencing ($n = 4$ for each time point per condition). (**B**) pH measurements of the growth media (mean ± SE, $n = 3$ biological replicates for each time point per condition, $^{***}P < 0.001$, nonsignificant (ns), two-sided Student's t test). (**C**) PCA. (**D**) Heatmap representation of genes that were significantly altered (see Methods) between time points within conditions. Data are presented as row z-scores of the expression per condition. See also S1 Fig and S1 Table. The data underlying the graphs shown in the figure is included in S1 Data. Graphical illustrations were generated with BioRender.com. PCA, principal component analysis.

https://doi.org/10.1371/journal.pbio.3002367.g001

CO_2 alters the expression of genes that participate in cholesterol biosynthesis

To identify potential transcription factors that participate in gene expression regulation in response to CO_2 or NaOH, we took an advantage of our time course analysis and performed unbiased cluster analysis (Fig 2A). We identified 3 major clusters; *Cluster 1*: Transcripts that were monotonically down-regulated (CO_2 or NaOH; 511 and 1,102, respectively); *Cluster 2*:

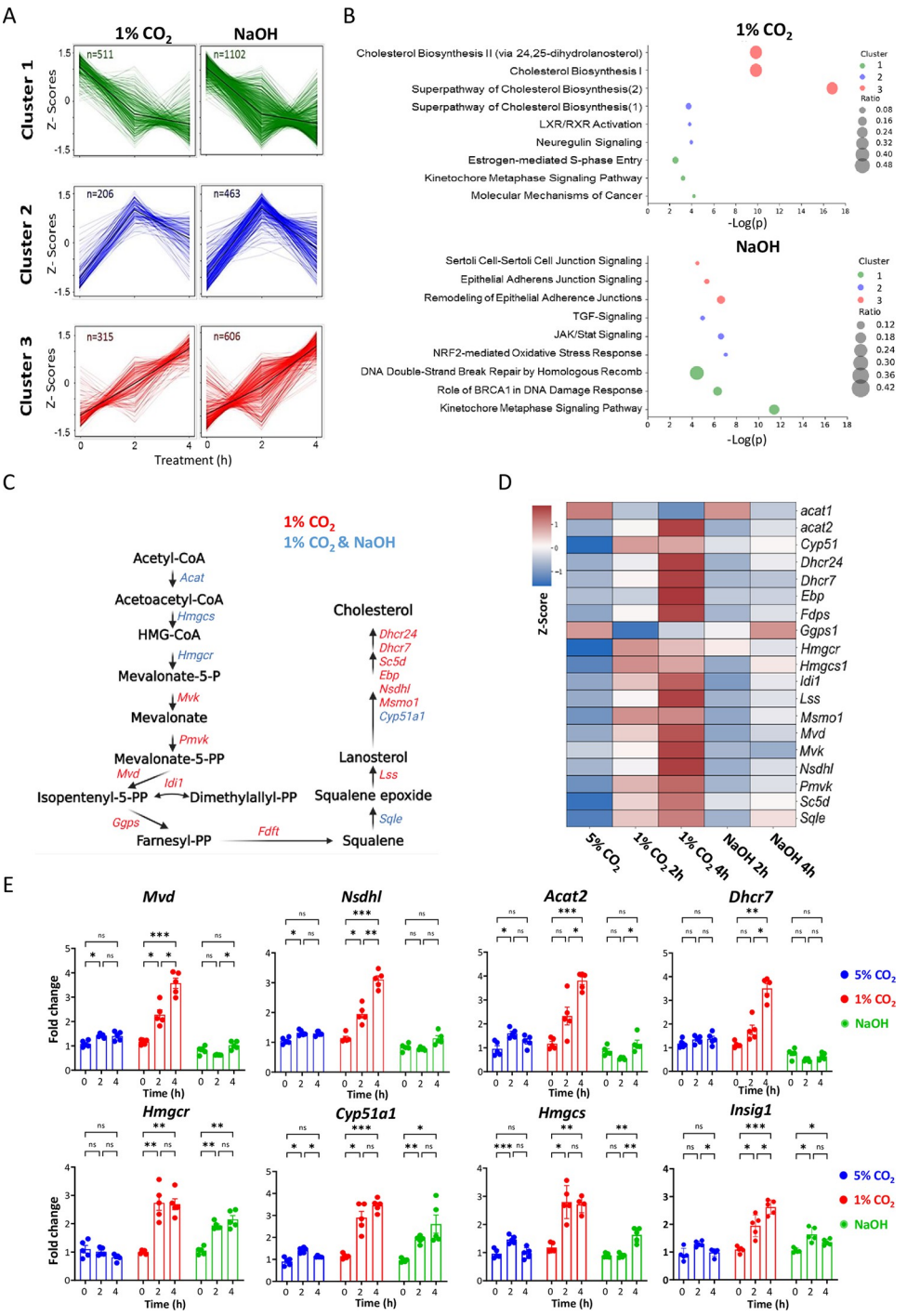

Fig 2. Low CO_2 levels specifically induce the expression of genes related to cholesterol biosynthesis. (A) K-means unsupervised clustering of significant genes for each of the conditions. Black line represents the mean z-score (for gene lists see S2 Table). **(B)** Pathway enrichment analysis was performed using the IPA tool for the genes included in each of the clusters for 1% CO_2 or 18 mM NaOH treatments. Presented are the top 3 enriched pathways in each cluster based on *P* value (for full list of pathways, see S3 Table). **(C)** Schematic illustration of the cholesterol biosynthesis pathway alongside genes that were significantly affected by the treatments. Color indicates on the condition in which the genes are affected. **(D)** Heatmap representation of cholesterogenic genes that were significantly affected by any of the conditions presented. Data are presented as row z-score of the average expression per condition ($n = 4$ biological replicates). **(E)** Quantitative PCR analysis of cholesterogenic gene expression levels from NIH3T3 cells treated with 1% CO_2 or 18 mM NaOH (mean ± SE, $n = 5$ biological replicates per time point per condition, $^{*}P < 0.05$, $^{**}P < 0.01$,

***$P < 0.001$, nonsignificant (ns), two-way ANOVA with Tukey's post hoc test) (see also S2 and S3 Figs and S2 and S3 Tables). The data underlying the graphs shown in the figure is included in S1 Data. IPA, ingenuity pathway analysis.

https://doi.org/10.1371/journal.pbio.3002367.g002

Transcripts that were up-regulated exclusively after 2 h (CO_2 or NaOH; 206 and 463, respectively); and *Cluster 3*: Transcripts that were monotonically up-regulated (CO_2 or NaOH; 315, and 606, respectively). Next, to uncover related biological processes affected by each treatment, we performed pathway enrichment analysis on each cluster. Remarkably, we found that cholesterol biosynthesis and its related processes are highly enriched in response to CO_2 but not to NaOH, specifically in cluster 3 which includes the monotonically up-regulated transcripts (Fig 2B). These findings indicated that low CO_2 induces the expression of genes implicated in cholesterol metabolism and that this effect is not a mere response to alkaline conditions, as it was not apparent upon NaOH treatment. This prompted us to specifically examine expression pattern of enzymes involved in de novo cholesterol biosynthesis based on our RNA-sequencing data. The vast majority of enzymes involved in different stages of cholesterol biosynthesis were up-regulated in cells exposed to low CO_2. Notably, the induction of these transcripts was mostly absent in NaOH-treated cells (Fig 2C and 2D). Furthermore, analysis of cholesterogenic gene expression by qPCR showed that in most cases their transcript levels are specifically induced by low CO_2 levels but not upon NaOH treatment (Fig 2E). These results were in line with the above detailed RNA-sequencing analysis. A similar trend was observed in hepatocyte murine cell line (Hepa1c1) (S2A Fig). In addition, these effects were recapitulated in primary tail fibroblasts and primary muscles, but not in primary white or brown adipocytes (S2A Fig).

Next, we examined the effect of hypercapnia, namely elevated CO_2 level, on cholesterogenic gene expression. Cells were exposed to increased CO_2 level (i.e., 10%) for 2 and 4 h and the transcript levels of cholesterogenic genes were analyzed by qPCR. Here again, O_2 level was maintained constant at 20% using our CO_2, O_2 and temperature-controlled chambers. High CO_2 levels elicited the opposite effect to lower CO_2 levels and the expression levels of cholesterogenic genes were suppressed (S2B Fig). Comparison of gene expression data of THP-1 monocytes exposed to 10% CO_2 [10] with our NIH3T3 cells data (1% CO_2 exposure) showed a small overlap in the responsive genes (S3A Fig). Yet, this small group included cholesterogenic genes (e.g., *Ldlr*, *Idi1*, *Insig1*, *Hmgcs1*, *Dhcr7*) and their response was in line with our findings, namely 10% CO_2 repressed of their expression (e.g., *Insig1*, *Hmgcs1*) (S3B Fig).

Taken together, our analyses reveal that alteration of CO_2 levels from the physiological range modulate the expression of genes involved in cholesterol homeostasis. Reduced and elevated CO_2 levels activate and repress their expression, respectively.

SREBP2 is activated in response to low CO_2 to induce the expression of cholesterogenic genes

SREBP2 is a key transcriptional regulator of genes involved in cholesterol biosynthesis [11,12]. In response to changes in cholesterol levels, SREBP2 translocates from the ER to the Golgi, where subsequent cleavage occurs and the N-terminal form of SREBP2 shuttles to the nucleus and activates the expression of transcripts involved in cholesterol biosynthesis [13]. Our transcription factor analysis predicted SREBP2 among the top potential transcriptional regulators for the expression of genes that are up-regulated (clusters 2 and 3) upon exposure to low CO_2 but not in response to NaOH treatment (Fig 3A and 3B).

We, therefore, hypothesized that SREBP2 is activated in response to low CO_2 to induce the expression of enzymes involved in cholesterol biosynthesis. To test this, cultured cells were exposed to low CO_2 and SREBP2 was analyzed by SDS-PAGE and immunoblot analysis. We

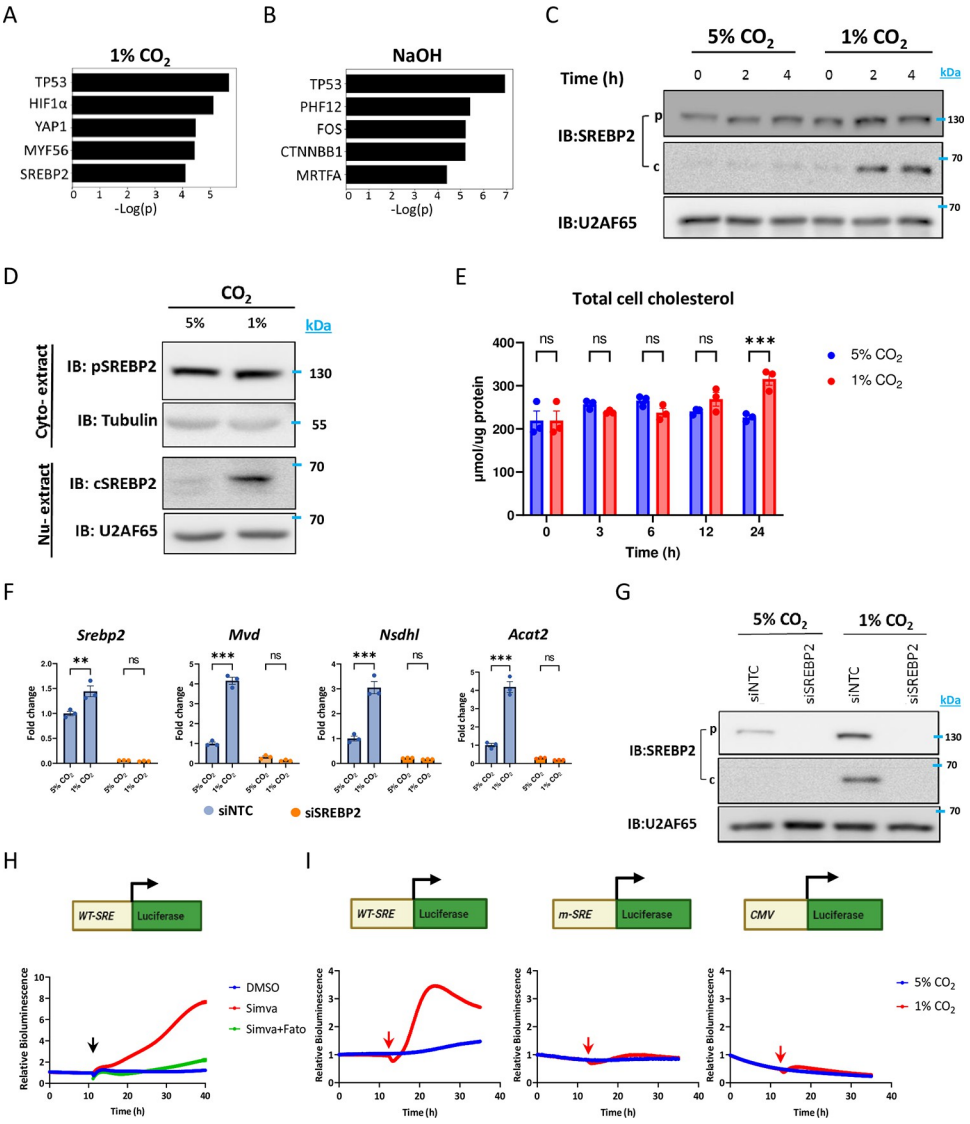

Fig 3. Low CO_2 levels activate SREBP2 and induce the expression of cholesterogenic genes through SRE. (A, B) Upstream regulator analysis was performed with IPA for clusters 2 and 3 within each condition. The top transcription factors, with the highest *p*-value, are presented (for full list, see S4 Table). **(C)** Immunoblot of total cell extracts from NIH3T3 cells exposed to either 5% CO_2 or 1% CO_2 p—SREBP2 precursor (approximately 126 kD); c—SREBP2 cleaved form (approximately 68 kD) (pooled sample of $n = 3$ biological replicates). **(D)** Immunoblot of cytoplasmic (Cyto-extract) and nuclear fractions (Nu-extract) from NIH3T3 cells exposed to either 5% or 1% CO_2 for 4 h (pooled sample of $n = 3$ biological replicates). **(E)** Total cholesterol quantification of NIH3T3 cells that were exposed to 5% or 1% CO_2 for 0, 3, 6, 12, 24 h (mean ± SE, $n = 3$ biological replicates per condition, $^{***}P < 0.001$, nonsignificant (ns), two-way ANOVA with Bonferroni's multiple comparisons test). **(F)** Quantitative PCR analysis for expression levels of cholesterol biosynthesis-related genes from control (siNTC) or SREBP2 silenced (siSREBP2) NIH3T3 cells exposed to 5% or 1% CO_2 for 4 h (mean ± SE, $n = 3$ biological replicates per condition, $^{***}P < 0.001$, $^{**}P < 0.01$, nonsignificant (ns), two-way ANOVA with Bonferroni's multiple comparisons test). **(G)** Immunoblot of NIH3T3 cells under the same condition as in **(F)** (pooled sample of $n = 3$ biological replicates). **(H)** Bioluminescence recordings from NIH3T3 cells transfected with SRE-Luc reporter plasmid (WT-SRE) and exposed to DMSO (control), 20 μm simvastatin or 20 μm simvastatin + 20 μm fatostatin, black arrow indicates the time of treatment (mean ± SE, $n = 3$ biological replicates per condition, AUC for control 1.14 ± 0.009, simvastatin 4.05 ± 0.06 ($P < 0.0001$), simvastatin + fatostatin 1.33 ± 0.04 ($P < 0.0001$), two-sided Student's *t* test). **(I)** Bioluminescence recordings from NIH3T3 cells transfected with WT SRE-Luc, mutant SRE-Luc, or control vector (CMV-Luc), and exposed to either 5% or 1% CO_2, the red arrow indicates the shift in CO_2 levels (mean ± SE, $n = 6$ biological replicates per condition, AUC for SRE Luc 5% CO_2 1.24 ± 0.03, 1% CO_2 2.77 ± 0.01 ($P < 0.0001$), mSRE Luc 5% CO_2 0.83 ± 0.02, 1% CO_2 0.91 ± 0.01 ($P < 0.002$), CMV Luc 5% CO_2 0.33 ± 0.007, 1% CO2 0.42 ± 0.01 ($P < 0.001$), two-sided Student's *t* test) (see also S4 and S5 Figs). The data underlying the graphs shown in the figure is included in S1 Data. AUC, area under curve; IPA, ingenuity pathway analysis; SRE, sterol regulatory element.

https://doi.org/10.1371/journal.pbio.3002367.g003

found that the cleaved form of SREBP2 (approximately 68 kD) accumulates 2 and 4 h following exposure to low CO_2 levels (Fig 3C). This effect was specific to low CO_2 and not to alkalic pH as it was not observed in NaOH-treated cells (S4A Fig). Biochemical nuclear-cytoplasmic fractionation further showed that the cleaved form of SREBP2 accumulates in the nucleus upon exposure to low CO_2 levels (Fig 3D). Together, our findings indicate that the SREBP2 signaling pathway is activated upon exposure to low CO_2 levels. To examine the functional consequence of SREBP2 and its downstream gene activation, we performed a time course analysis (0, 3, 6, 12, and 24 h) and measured cholesterol levels in cells cultured either at 5% or 1% CO_2. Upon 24 h exposure to low CO_2 levels, cells accumulated cholesterol, in line with SREBP2 activation and elevated the expression of cholesterogenic genes (Fig 3E). Next, we asked whether the induction of cholesterogenic genes under low CO_2 is SREBP2-dependent. To this end, cells were transfected with either control siRNA (siNTC-Non Template Control) or siRNA against mouse SREBP2 (siSREBP2) and were exposed either to 1% CO_2 or 5% CO_2 for 4 h. As expected, SREBP2 was undetectable in siSREBP2-silenced cells under both 5% and 1% CO_2 and the basal expression levels of SREBP2 target genes was lower (Fig 3F and 3G). Control cells showed accumulation of the cleaved form of SREBP2 upon 1% CO_2 as well as induction of its cholesterogenic target genes (Fig 3F and 3G). Importantly, the induction of cholesterogenic genes was completely abolished in SREBP2 silenced cells under low CO_2 levels, indicating that the effect is SREBP2-dependent (Fig 3F). We also identified several transcripts that are induced upon low CO_2 levels in our gene expression analysis yet their induction was SREBP2-independent (S4B Fig). It is conceivable that the response to low CO_2 levels is coordinated through the concerted action of several transcription regulators and is not exclusively SREBP2-dependent. Overall, our results suggest that low CO_2 levels elicit SREBP2 cleavage and nuclear accumulation to induce the expression of its target genes, primarily cholesterogenic genes and consequently cholesterol accumulation.

Low CO_2 activates gene expression through a sterol regulatory element

SREBP2 activates the transcription of its downstream targets by binding to a specific region on the promoter sequence known as sterol regulatory element (SRE) [14]. To examine whether low CO_2 levels can activate gene expression through an SRE, we employed an SRE reporter assay. This reporter is based on the HMG-CoA synthase promoter sequence harboring SRE that drive the expression of a firefly luciferase [15]. Cells were transfected with the SRE reporter and bioluminescence was continuously monitored. Consistent with the activation of SRE by SREBP2, treatment with simvastatin, which inhibits de novo cholesterol biosynthesis [16] and activates SREBP2, resulted in increased bioluminescence. This effect was suppressed upon co-administration of fatostatin (Fig 3H), which inhibits SREBP2 ER-to-Golgi translocation [17].

Then, we tested the effect of low CO_2 on the reporter activity. In line with above-described findings, a decrease in CO_2 levels from 5% to 1% induced an increase in bioluminescence of cells expressing the wild-type reporter (pSynSRE-T-Luc) (Fig 3I). A decrease in CO_2 levels had no effect on the bioluminescence of cells expressing either a mutant reporter (pSynSRE-Mut-T-Luc) [18] or a control luciferase reporter (pcDNA3-Luc) (Fig 3I). Consistently, an increase in CO_2 levels from 5% to 10% markedly suppressed the bioluminescence from cells expressing a wild type but not a control luciferase reporter (S5A Fig).

In our bioluminescence reporter assays, we observed an initial minor response that was not SRE-specific and was evident in the control reporters as well. This unspecific response likely stems from the effect of pH changes on bioluminescence in general [19].

Next, we employed our reporter assay to examine whether SRE activation by low CO_2 is reversible. To this end, cells expressing wild-type SRE reporter were exposed to either constant

5% as a control or interchanging 5% to 1% CO_2 levels and bioluminescence was continuously recorded. A shift in CO_2 levels from 5% to 1% increased the bioluminescence levels. This increase was reduced back to basal levels once CO_2 levels were shifted to 5% (S5B Fig). This result indicates that CO_2 reversibly modulate SRE activation and likely SREBP2 activation.

Taken together, our results suggest that an intact SRE is sufficient for the transcriptional response to changes in CO_2 levels and the effects of CO_2 levels on it are reversible.

Stability of the mature cleaved form of SREBP2 is not affected by low CO_2 levels

SREBP2 translocates from the ER-to-Golgi and subsequently reaches the nucleus to induce gene expression. The exit of SREBP2 from the ER is regulated by sterol levels via SREBP cleavage-activating protein (SCAP) and insulin-induced gene (INSIG). Low ER cholesterol levels destabilize INSIG-SCAP interaction and successively enable the SREBP2-SCAP complex to translocate from the ER to Golgi where SREBP2 is cleaved [20]. The mature N-terminal cleaved form of SREBP2 then shuttles to the nucleus [13] to activate gene expression as aforementioned through SRE sites on target genes [21].

Hitherto, we showed that upon low CO_2 levels SREBP2 is cleaved, the N-terminal cleaved form accumulates in the nucleus and can activate gene expression though an intact SRE site (Fig 3). To identify the signaling node though which SREBP2 is activated in response to low CO_2 levels, we systematically examined the different steps in the SREBP2 signaling pathway (S6A Fig) comparing sterol depletion with exposure to low CO_2 levels.

In the nucleus, the levels of mature cleaved form of SREBP2 are regulated by its proteasomal degradation [22] as stabilization of the nuclear form by proteasome inhibition or defective polyubiquitination actively induce its target genes [23,24]. We hypothesized that low CO_2 levels might alter nuclear SREBP2 turnover and thereby induce its nuclear accumulation and target gene expression. To test this, we exogenously expressed in cultured NIH3T3 cells a FLAG-tagged truncated mature SREBP2 fragment (FLAG N-SREBP2) [25], which was shown to localize in the nucleus [26]. Cells were exposed either to sterol depletion upon methyl-β-cyclodextrin (MBCD) treatment or to 1% CO_2 levels. Total protein extracts were prepared and analyzed by immunoblot with either anti-SREBP2 or anti-FLAG antibody to detect the endogenous or the exogenously expressed truncated forms, respectively. Both MBCD treatment and exposure to low CO_2 induced the accumulation of the endogenous cleaved form of SREBP2 (S6B Fig). However, neither treatment affected the levels of the exogenously expressed cleaved form (i.e., FLAG N-SREBP2) (S6C Fig), suggesting that low CO_2 levels, similar to sterol depletion by MBCD do not affect the nuclear stability of the cleaved mature form of SREBP2.

Low CO_2 levels induce the ER-to-Golgi translocation of SREBP2

SCAP-SREBP2 ER-to-Golgi translocation is a critical step in SREBP2 activation and subsequent induction of its target genes. To examine whether the activation of SREBP2 upon low CO_2 is dependent on its ER-to-Golgi trafficking, we employed fatostatin, which pharmacologically blocks the ER-to-Golgi transport of SCAP-SREBP2 [17]. Cells were exposed to either fatostatin or DMSO as control under 5% or 1% CO_2. Low CO_2 levels induced the accumulation of the mature cleaved form of SREBP2. Importantly, this effect was blocked in the presence of fatostatin (S6D Fig). Consistently, the induction of SREBP2 target genes in response to low CO_2 levels was eliminated in the presence of fatostatin (S6E Fig). This result indicated that ER-to-Golgi trafficking is necessary for activation of SREBP2 by low CO_2 levels.

As aforementioned, SCAP regulates SREBP2 transport in a sterol-dependent fashion as it retains the SCAP-INSIG-SREBP2 complex in the ER membrane and inhibits the subsequent processing of SREBP2, namely, its cleavage and ER-Golgi translocation [27]. We, therefore, examined whether activation of SREBP2 by low CO_2 levels is also SCAP-sensitive. We employed siRNA to knockdown SCAP and exposed control (siNTC) or SCAP knockdown (siSCAP) cells to low CO_2 levels (i.e., 1%). Low SCAP levels in cultured cells were shown to suppress SREBP2 proteolysis and expression of SREBP2 downstream target genes [28,29]. The induction of SREBP2 target genes in response to low CO_2 levels was as well suppressed in SCAP-deficient cells likely due to inhibition of SREBP2-SCAP ER-to-Golgi translocation (S6F Fig).

Together, our analyses suggest that activation and induction of SREBP2 target genes upon low CO_2 levels is dependent on ER-to-Golgi trafficking and regulated by SCAP. Hence, it seems to follow the canonical pathway of SREBP2 activation as in response to low sterol levels.

Low CO_2 levels reduces ER cholesterol levels

The main driver of SREBP2 signaling pathway is reduction in ER cholesterol levels. Hitherto, activation of SREBP2 by low CO_2 levels followed similar steps in the canonical SREBP2 pathway as upon sterol depletion. These findings raised the following questions: (i) Does SREBP2 activation by low CO_2 levels depend on cellular cholesterol levels; and (ii) do CO_2 levels affect cellular cholesterol levels?

First, we examined if SREBP2 activation by low CO_2 levels is affected by cellular cholesterol levels. To this end, we exposed cells expressing the SRE reporter to increasing concentrations of MBCD to deplete cholesterol while shifting CO_2 levels from 5% to 1% (Fig 4A). In line with the above, both sterol depletion under 5% CO_2 as well as exposure to 1% CO_2 levels, increased the bioluminescence of the SRE reporter (Fig 4B). Up to 5 mM MBCD, we observed an additive effect in response to 1% CO_2. Whereas in the presence of higher levels of MBCD, namely, 7 mM, low CO_2 levels elicited a very minor effect on the activation of the SRE reporter (Fig 4B). The diminished effect of low CO_2 upon elevated levels of MBCD and likely highly depleted cholesterol levels, raised the possibility that low CO_2 levels activate SREBP2 in a cholesterol-dependent manner.

To directly examine whether low CO_2 affected cellular cholesterol levels, we first quantified total cholesterol levels in cells exposed to 5% or 1% CO_2 for 4 h or upon MBCD treatment. As expected in MBCD treated cells, we observed a marked reduction in total cholesterol levels. By contrast, low or high CO_2 levels did not show any significant effect on total cellular cholesterol (Figs 4C and S7A, respectively).

SREBP2 is specifically activated in response to changes in ER sterol levels [30]. Furthermore, changes in ER cholesterol levels are sufficient to activate SREBP2 even if total cholesterol levels are unaltered [31]. This prompted us to examine whether CO_2 alterations specifically affect ER cholesterol levels. Hence, we repeated the above-described experiment, but this time ER membranes were isolated through differential centrifugation, with subsequent sucrose gradient and OptiPrep separation, as previously described [30]. ER membrane free cholesterol and cholesterol ester content were quantified (Fig 4D and 4E). MBCD treatment significantly reduced ER cholesterol (Fig 4D), consistent with previous reports [30,31]. Remarkably, although low CO_2 levels did not affect total cellular cholesterol, we observed a substantial decrease in ER free cholesterol levels (Figs 4D and S7D). No significant effect on cholesterol esters content was detected (Figs 4E and S7D).

Cholesterol or 25-hydroxylcholesterol supplementation elevates the ER cholesterol pool that acts through SCAP-Insig binding to anchor SREBP2 in the ER and inhibit its activation

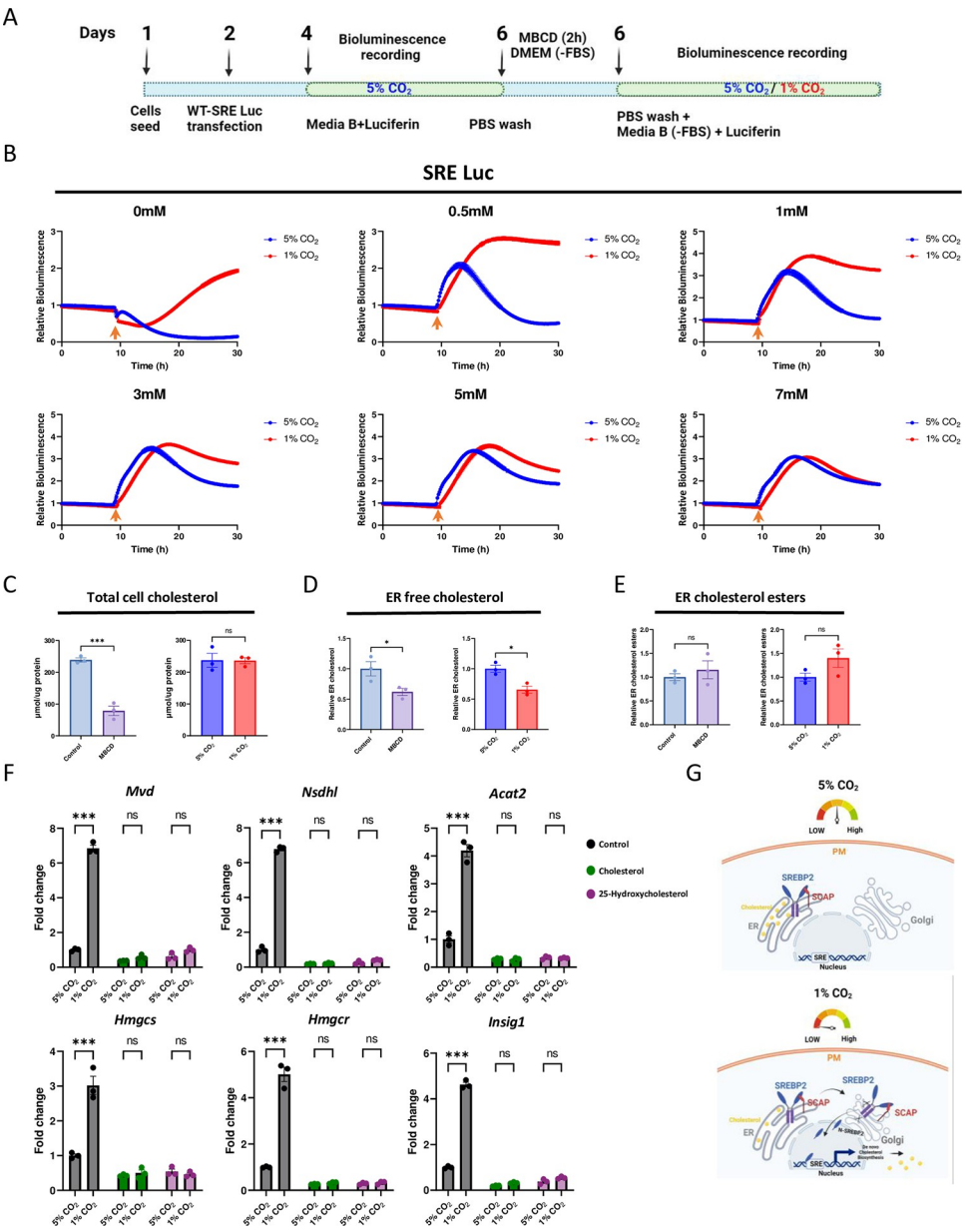

Fig 4. Exposure to low CO_2 levels decreases ER cholesterol levels. (A) Schematic depiction of the experimental design. NIH3T3 cells transfected with reporter plasmid were treated with different MBCD concentrations for 2 h, followed by exposure to either 5% or 1% CO_2, and bioluminescence levels were continuously recorded in a medium B (without serum) containing luciferin. **(B)** Bioluminescence recordings from the different conditions as depicted in **(A)**, the arrow indicates the time CO_2 was shifted from 5% to 1% (mean ± SE, $n = 4$ biological replicates per condition, AUC for 0 mM 0.34 ± 0.007, 1.59 ± 0.004 ($P < 0.0001$), 0.5 mM 1.00 ± 0.023, 2.68 ± 0.04 ($P < 0.0001$), 1 mM 1.66 ± 0.07, 3.34 ± 0.04 ($P < 0.0001$), 3 mM 2.06 ± 0.02, 2.79 ± 0.07 ($P < 0.0001$), 5 mM 2.02 ± 0.05, 2.43 ± 0.06 ($P < 0.002$), 7 mM 1.85 ± 0.01, 1.77 ± 0.02 ($P < 0.02$) two-sided Student's t test). **(C)** Total cholesterol quantification (with fluorometric assay kit) in NIH3T3 cells depleted with sterols for 2 h or exposed to different CO_2 levels for 4 h (mean ± SE, $n = 3$ biological replicates per condition, $^{**}P < 0.01$, nonsignificant (ns), two-sided Student's t test). **(D, E)** The free cholesterol and cholesterol ester levels in the ER membrane from the cells as in **(C)**, were quantified with shotgun lipidomics analysis (see S7 Fig and S5 Table) (mean ± SE, $n = 3$ independent experiments, $^{**}P < 0.01$, $^{*}P < 0.05$, nonsignificant (ns) two-sided Student's t test). **(F)** qPCR analysis for cholesterogenic genes from NIH3T3 cells exposed to cholesterol (50 μm) or 25-hydroxycholesterol (10 μm) under 5% or 1% CO_2 for 4 h (mean ± SE, $n = 3$ biological replicates per condition, $^{***}P < 0.001$, nonsignificant (ns), two-way ANOVA with Bonferroni's multiple comparisons test). **(G)** A schematic model; in cells under normal physiological CO_2 levels (5%) ER cholesterol levels are unaffected and SREBP2 is retained in the ER membrane. However, under low CO_2 levels (1%), ER cholesterol levels are decreased, inducing SREBP2 activation and subsequent activation of cholesterol biosynthesis related genes

through SRE region on their gene promoter. The data underlying the graphs shown in the figure is included in S1 Data. Graphical illustrations were generated with BioRender.com. AUC, area under curve; ER, endoplasmic reticulum; MBCD, methyl-beta-cyclodextrin; SRE, sterol regulatory element.

https://doi.org/10.1371/journal.pbio.3002367.g004

[32]. To examine the effect of ER cholesterol pools, cells were exposed to low CO_2 in presence of cholesterol or 25-hydroxycholesterol for 4 h and the expression of cholesterogenic genes was analyzed. The transcriptional response of cholesterogenic genes to low CO_2 was abolished in presence of cholesterol or hydroxycholesterol, which further supports involvement of cholesterol levels and most likely ER cholesterol on SREBP2 activation under low CO_2 (Fig 4F).

In summary, our analyses suggest that low CO_2 specifically alters ER cholesterol, and this effect likely triggers the subsequent processing and activation of SREBP2.

Discussion

Alterations in CO_2 levels (hypocapnia or hypercapnia) have been increasingly linked to various pathologies [6,33–35], yet the molecular mechanisms that are implicated in the response to changes in CO_2 remain elusive.

In the present study, we show that a decrease in CO_2 levels activate a distinct gene expression program that differs from mere pH changes (e.g., NaOH treatment). These findings support the presence of a specific mechanism that respond to changes in CO_2 levels. Furthermore, we show that SREBP2 participates in CO_2 signaling to regulate the expression of its target genes, primarily genes of cholesterol biosynthesis. Of note, CO_2 is in equilibrium with HCO_3^-, hence, we cannot conclude whether the observed cellular response to altered CO_2 is due to molecular CO_2 or to changes in bicarbonate levels. Dissecting the effect of CO_2 per se from associated change in bicarbonates is expected to be challenging in view of their rapid equilibrium in physiological systems. This issue can be potentially addressed by using out-of-equilibrium CO_2/HCO_3^- solutions [36]. In addition, manipulation of CO_2 levels in vivo in animal models are extremely challenging due to various homeostatic mechanisms that rapidly act to maintain the equilibrium between CO_2, bicarbonate, and pH levels.

Interestingly, in pancreatic cancer cells SREBP2 induces the expression of cholesterogenic genes in response to extracellular acidic condition [37]. Consistently, our results show that alkaline conditions per se (i.e., NaOH treatment), unlike exposure to low carbon dioxide levels, elicit a minor effect on the expression of SREBP2 target genes in non-cancerous cells. Hence, it appears that SREBP2 can be activated in response to various stimuli, namely low carbon dioxide levels and acidic conditions. Since low carbon dioxide levels are associated with alkaline and not acidic conditions, it further supports our conclusion that low CO_2 levels activate SREBP2 through distinct mechanism that is not necessarily pH-related. It is noteworthy that different cell types might respond differently to pH or CO_2 levels. Previous reports showed that carbon dioxide regulates different signaling pathways such as NFκB, Wnt, and TGFβ signaling, as well as circadian rhythms in different cell types [10,38–40]. We also show that SREBP2 is activated in response to low CO_2 levels in fibroblast, hepatocytes, and muscles but not in adipocytes. Hence, it is conceivable that the response to CO_2 is conducted through myriad of signaling pathways, some of which are cell-type specific. Our gene expression analysis identified HIF-1α and YAP as potential candidates that participate in the response to CO_2. Indeed, hypoxia regulates cholesterol metabolism through HIF-1α [41], yet the involvement of HIF-1α in conjunction with SREBP2 in response to CO_2 was hitherto never tested. Likewise, recent evidence points towards functional interaction between YAP and SREBP in regulation of lipid metabolism [42,43]; however, its relevance to CO_2 remains unknown.

Importantly, a role of CO_2 in the control of cholesterol homeostasis has not been previously reported. Interestingly, cellular cholesterol has been shown in vitro to regulate CO_2 permeability in different cell types [44,45]. In these studies, each cell type exhibited different CO_2 permeability rate depending on its cholesterol content [45]. This raises the intriguing possibility of a mechanism whereby changes in CO_2 levels regulate cholesterol biosynthesis through SREBP2 to regulate cell membrane cholesterol content and control CO_2 permeability in response to environmental changes.

Although, CO_2 is generated as a byproduct of cellular enzymatic reactions, CO_2 is also consumed as a carbon source in the conversion of acetyl-CoA to malonyl-CoA. Acetyl-CoA serves as a key precursor for both fatty acid and cholesterol biosynthesis pathways that are major lipid building blocks for cell membranes. SREBPs control the flux of acetyl-CoA into fatty acid and mevalonate synthetic pathways [46]. Reduction of extracellular CO_2 might limit the abundance of intracellular CO_2 and would shift the flux of acetyl-CoA towards cholesterol biosynthesis. This shift in substrate supply may serve to support the increased expression of cholesterogenic enzymes by SREBP2.

At the molecular level, our findings suggest that under physiological growth conditions (i.e., 5% CO_2), SREBP2 is retained in the ER membrane. Low CO_2 reduces ER cholesterol levels and triggers SREBP2 translocation from ER to Golgi, where SREBP2 is cleaved. The cleaved, transcriptionally active form of SREBP2 (N-SREBP2) enters the nucleus and activates transcription of cholesterol biosynthetic enzymes through SRE region on the gene promoter (Fig 4G). It remains unclear how CO_2 modulates the ER lipids composition, and future studies are expected to address the underlying molecular mechanisms.

In summary, we propose that SREBP2 participates in cellular CO_2 signaling and that SREBP2 regulation of cholesterol levels can be modulated by changes in CO_2 levels.

Methods

Ethics statement

All animal experiments and procedures were conducted in conformity with and approval of the Weizmann Institute Animal Care and Use Committee (IACUC) guidelines, working within the anti-cruelty law (experiments on animals) of 1994 as stated by the Ministry of Health of the Israeli Parliament. Experiments were done in accordance with these specific applications: 05730621–1 and 01700223–2.

Cell culture

NIH3T3, Hepa1c1 cells were routinely cultured in media A (DMEM with high glucose (01-052-1A, Biological Industries) supplemented with 10% FBS, 100 units/ml penicillin, 100 mg/ml streptomycin, 44 mM $NaHCO_3$) at 37˚C in a humidified incubator with 5% CO_2. Mouse tail tip fibroblasts (TTFs) were routinely cultured as previously described [47] with media A containing 20% FBS. Mouse primary muscles were isolated and cultured as previously described [48] with BioAmf2 (Biological Industries Cat # 01-194-1A) and were differentiated in DMEM: F12 (Sigma D6421) supplemented with 2% Horse Serum (04-004-1A, Biological Industries). Fully differentiated fibers were used for the experiment. Mouse white and brown adipocytes were isolated, cultured, and differentiated as previously described [49]. All the experiments were performed in media B (Bicarbonate free DMEM (5×, 01-055-4A Biological Industries) diluted to 1× with deionized water and supplemented with 10% FBS, 4 mM L-Glutamine, 100 units/ml penicillin, and 100 mg/ml streptomycin with 18 mM sodium bicarbonate).

Reagents and chemicals

Reagents and drugs used are listed in S6 Table. Information regarding dosage and solvents are detailed in the relevant figure legends.

Plasmids and siRNA transfections

The plasmids pcDNA3.1-2xFLAG-SREBP-2 (#26807), pSynSRE-T-Luc (#60444), pSynSRE-Mut-T-Luc (#60490), pcDNA3-Luciferase (#18964) were purchased from Addgene. The siRNA against mouse SREBP2 (L-050073-01-0010), SCAP (L-040322-01-0010), and control (D-001810-10-50) were purchased from Dharmacon. Briefly, 2.5×10^5 cells were seeded in 3-cm culture dish in media B. For plasmid transfection, in the next day cells were transiently transfected with the 750 ng of the indicated plasmids using jetPRIME (Polyplus) as per the supplier protocol. Alternatively, for siRNA treatment, cells were transfected with 25 nM siRNA using Lipofectamine RNAiMAX (Thermo Fisher Scientific) transfection reagent with 1:3 siRNA/reagent ratio. Cells were analyzed 48 h after transfection by either immunoblot, qPCR, or bioluminescence assays unless indicated otherwise.

RNA extraction and qPCR analysis

RNA extraction from the cells were performed by TRI-reagent (Sigma) with manufacturer standard protocol. RNA concentration was determined using NanoDrop2000 Spectrophotometer (Thermo Fisher Scientific, USA). RNA integrity was validated using 2200 TapeStation (Agilent, USA). Synthesis of cDNA was performed using qScript cDNA SuperMix (Quanta Biosciences). Real-time PCR measurements were performed using SYBR green primers with LightCycler II machine (Roche) and normalized to the geometrical mean of 3 housekeeping genes (*Rplp0*, *Tbp*, and *Hprt*). Primer sequences are listed in S7 Table.

RNA sequencing

Bulk MARS-seq libraries [50] were prepared from the mRNA extracted from NIH3T3 cells untreated or exposed to either 1% CO_2 or 18 mM NaOH under 5% CO_2 for 0, 2, and 4 h, and subsequently sequenced with high-output 75-base-pair kits (catalogue no. FC-404-2005; Illumina, USA) on a NextSeq 550 Illumina sequencer.

RNA-sequencing data analysis

Processing of raw sequencing data into read counts was performed via Transcriptome Analysis Pipeline (v.1.10) [51]. In short, reads were trimmed using cutadapt (v.1.15) [52] and mapped to the genome (/shareDB/iGenomes/Mus_musculus/UCSC/mm10/Sequence/STAR_index) using STAR (v.2.5.2b) (default parameters) [53]. The pipeline quantifies the genes annotated in RefSeq that have extended with 1,000 bases towards the 5′ edge and 100 bases towards the 3′ bases. Unique molecular identifier (UMI) counts were done using HTSeq-count (v.0.9.1) in union mode [52]. Normalization of the counts was performed using DESeq2 (v.1.16.1) with the betaPrior = True, cooksCutoff = FALSE, independentFiltering = FALSE parameters [54].

RNA-seq data are available from the GEO database (accession number GSE196294). All other data that support the findings of this study are available upon request.

Pathway enrichment and upstream transcription factor analysis

Enrichment analysis and upstream transcription factor analysis was performed with Ingenuity Pathway Analysis software QIAGEN IPA (QIAGEN) with default setting.

Sterol depletion

Sterol depletion from the cells was performed by MBCD (Sigma) treatment. Cells were seeded in media B at density 300,000 cells/3 cm dish. On day 4, cells were washed with PBS twice to remove residual serum and cells were incubated in DMEM (Gibco, 21063–029) without serum, supplemented with either 2 mM MBCD (100 mM stock in water) or vehicle control for 2 h at 37˚C and 5% CO_2. Next, cells were washed twice with PBS and cultured in media B without serum.

Bioluminescence recordings

Unless indicated otherwise, for bioluminescence recordings cells were seeded in media B at density of 300,000 cells per 3-cm culture dish. Next day, cells were transiently transfected with one of the plasmids containing pSynSRE-T-Luc (750 ng), pSynSRE-Mut-T-Luc (750 ng), or pcDNA3-Luc (500 ng) as detailed above. After 48 h from transfection, the culture medium was replaced with media B supplemented with 100 nM D-Luciferin (Promega, USA) and bioluminescence was recorded continuously with LumiCycle32 recorder (Actimetrics, USA) in a 37˚C, 5% CO_2 incubator. After 24 h (once the luciferase signal reached a stationary phase), CO_2 levels were shifted to 1%, 10%, or kept at 5% CO_2 as control. Bioluminescence data were extracted using the LumiCycle Analysis software (Actimetrics, USA). The relative bioluminescence was calculated by normalizing the raw counts to the 10 h pretreatment average value.

Protein extraction, gel electrophoresis, and immunoblotting

Whole cell lysate was prepared as previously described [9]. For nuclear and cytoplasmic fraction, cell pellets were resuspended in lysis buffer (HEPES 10 mM (pH 7.5), 10 mM KCl, 0.1 mM EDTA, 0.5% Noniodate 40, 1 mM DTT, PMSF 0.5 mM) supplemented with protease inhibitor cocktail (Sigma) and allowed to swell on ice for 15 to 20 min with intermittent mixing. Tubes were vortexed (10 s) to disrupt the cell membrane and then centrifuged at 12,000 g at 4˚C for 30 s. The supernatant was stored at −80˚C till further use as cytoplasmic extract. The pelleted nuclei were washed twice with 1 ml lysis buffer and was resuspended in nuclear extraction buffer (20 mM HEPES (pH 7.5), 400 mM NaCl, 1 mM EDTA, and 1 mM PMSF) with protease inhibitor cocktail and then incubated on ice for 30 min. Nuclear extracts were collected by centrifugation at 12,000 g for 15 min at 4˚C. The protein concentration of the cytoplasmic and nuclear extract was quantified using BCA protein assay kit (Thermo Scientific, USA). Finally, samples were heated at 95˚C for 5 min in Laemmli sample buffer and analyzed by SDS-PAGE and immunoblot. SREBP2 antibody that was used in our study (Anti-SREBP2, Clone 22D5, MABS1988, Lot # 3272232, Merck) recognizes the N-terminal region of murine SRE-binding protein 2. Details of the antibodies used are listed under S8 Table.

ER membrane isolation

Cells were seeded in 15-cm culture dish at density of 2×10^6 cells per dish. On day 4, cells were subjected to different treatments as indicated. Next, cells were washed with cold PBS, scrapped in 2 ml PBS, and collected in 15 ml tube. The suspension was centrifuged at 500 g for 10 min to obtain cell pellet, snap frozen in liquid nitrogen, and stored at −80˚C until further use. Isolation of ER membranes was performed with minor modification as previously described [30]. Cell pellet were homogenized with glass dounce (15 to 25 rounds) in cold lysis buffer (50 mM Tris-HCl (pH 7.5), 150 mM NaCl, 15% sucrose) containing protease inhibitor cocktails. A small aliquot of homogenate was stored as whole cell lysate (fraction A) (S7B Fig). The lysates were centrifuged at 3,000 g for 10 min to yield nuclear pellet and supernatant (fraction B).

Nuclear pellets were lysed with nuclear extraction buffer (20 mM HEPES (pH 7.5), 400 mM NaCl, 1 mM EDTA, and 1 mM DTT) and stored as fraction C. Further, the supernatant was diluted to 3 ml with lysis buffer and loaded on discontinuous sucrose gradient which was set in SW41 tube (Beckman) by overlaying the following sucrose solutions all in the above lysis buffer: 2 ml 45%, 4 ml 30%, 3 ml of the diluted supernatant in 15% sucrose, and 1 ml 7.5%. The tubes were ultra-centrifuged in SW41Ti rotor (Beckman) at 100,000 g for 60 min and allowed to slow down without application of a break. The 2 bands of membranes were clearly visible, upper light membrane fraction (Interphase between 15% and 7.5%) were collected and marked as fraction D and heavy membrane fraction (interphase between 45% and 30% sucrose) were collected in another tube as fraction E. The collected fractions at each stage were analyzed by immunoblot with relevant organelle markers as indicated (S7C Fig). Further, purification of heavy membrane fraction (fraction E) was performed with OptiPrep-Density gradient medium (Sigma). Fraction E from the above sucrose gradient was loaded at the bottom of SW41 tube and subsequently, overlaid with dilutions of OptiPrep-Density gradient medium. Discontinuous OptiPrep gradient was generated by underlying in sequence form bottom to top—1 ml fraction E, 2.5 ml each of 25%, 23%, 21%, 19% OptiPrep media diluted in ice cold tris-buffer (50 mM Tris-HCl (pH 7.5), 150 mM NaCl) and equilibrate for 2 h at 4˚C. After incubation, tubes were ultra-centrifuged at a speed of 110,000 g for 120 min. After centrifugation, OptiPrep fractions were collected from top to bottom of the tube (approximately 900 μl each fraction) and fractions were run on the SDS-PAGE with marker protein for ER membrane and the fraction showing no organelle contamination (fraction no 5) was used for lipidomic analysis.

ER-lipidomic analysis

Cholesterol and cholesterol ester were identified and quantified using multi-dimensional mass spectrometry-based shotgun lipidomic analysis [55]. In brief, each 300 μl ER suspension sample was accurately transferred to a disposable glass culture test tube. A pre-mixture of internal standards (IS) was added prior to conducting lipid extraction for quantification of the targeted lipid species based on the protein content of individual ER suspension. Lipid extraction was performed using a modified Bligh and Dyer procedure [56], and each lipid extract was reconstituted in chloroform:methanol (1:1, *v*:*v*) at a volume of 100 μl/300 μl ER suspension samples.

For shotgun lipidomics, lipid extract was further diluted to a final concentration of approximately 500 fmol total lipids per μl. Mass spectrometric analysis was performed on a triple quadrupole mass spectrometer (TSQ Altis, Thermo Fisher Scientific, USA) and a Q Exactive mass spectrometer (Thermo Scientific, USA), both of which were equipped with an automated nanospray device (TriVersa NanoMate, Advion Bioscience Ltd., Ithaca, NY) as described [57]. Identification and quantification of cholesterol and cholesterol ester were performed using an automated software program [58,59]. Data processing (e.g., ion peak selection, baseline correction, data transfer, peak intensity comparison, and quantitation) was performed as described [59]. The results were normalized to volume of ER suspension (pmol/100 μl ER suspension).

Total cholesterol quantification

Lipid extraction and cholesterol quantification were performed using a Total Cholesterol Assay Kit Fluorometrically (Cell Biolabs, STA-390) according to the manufacturer's protocol.

Statistics

All the statistical analyses were performed using Excel, Python, and GraphPad prism (Version 9.1.0.221). Specific information on sample sizes, statistical significance, and variance measures

is provided in the relevant figure legends. Significantly expressed genes are defined based on the difference in expression between each of the time points (i.e., T0, T2, T4) per condition, based on the following criteria: P adj. < = 0.05, |log2FC| > = 1, baseMean > = 5. Normalized data of significant genes in each of the conditions was clustered using Python's scikit-learn KMeans function. PCA analysis was performed using R's prcomp function (scale = TRUE) of stats package.

Supporting information

S1 Fig. Transcriptional response to low CO_2 levels compared to NaOH treatment. (A) Bar plot representing the number of significant genes (see Methods) that were up- or down-regulated in response to 1% CO_2 or 18 mM NaOH after 2 or 4 h exposure. **(B)** Venn diagrams representing the number of genes that significantly responded to 1% CO_2 or 18 mM NaOH after 2 or 4 h and their overlaps. The data underlying the graphs shown in the figure is included in S1 Data.
(TIF)

S2 Fig. Low CO_2 levels induce the expression of cholesterol biosynthesis related genes. (A) Quantitative PCR analysis of cholesterogenic gene expression levels from mouse Hepa1c1, primary tail tip fibroblasts (TTF), mouse primary muscles, white adipocytes (WAT), and brown adipocytes (BAT) cultured either at 5% CO_2 or 1% CO_2 for 4 h (mean ± SE, $n = 3$ biological replicates for Hepa1c1, $n = 3$ biological replicates per condition for TTF, muscles, WAT and BAT, $^{***}P < 0.001$, $^{**}P < 0.01$, $^{*}P < 0.05$, nonsignificant (ns), two-way ANOVA with Bonferroni's multiple comparisons test). **(B)** Quantitative PCR analysis of cholesterogenic gene expression levels from NIH3T3 cultured either at 5% CO_2 or 10% CO_2 for 2 or 4 h (mean ± SE, $n = 3$ biological replicates for each time point per condition, $^{***}P < 0.001$, $^{**}P < 0.01$, $^{*}P < 0.05$, nonsignificant (ns), two-way ANOVA with Bonferroni's multiple comparisons test). The data underlying the graphs shown in the figure is included in S1 Data.
(TIF)

S3 Fig. Comparative analysis of gene expression data from cells exposed to different CO_2 levels. (A, B) Gene expression data (Phelan and colleagues) of THP-1 monocytes exposed to 10% CO_2 for 4 h was compared with data of NIH3T3 exposed to 1% CO_2 for 2 h and 4 h. **(A)** A Venn diagram presentation of the overlap in the responsive genes from both datasets. **(B)** A bar graph presentation of the transcriptional response of common genes (28 for 2 h and 47 for 4 h). The data underlying the graphs shown in the figure is included in S1 Data.
(TIF)

S4 Fig. SREBP2 is activated in response to low CO_2 levels but not in response to alkaline conditions. (A) Immunoblot of total cell extracts from NIH3T3 cells exposed to either 5% CO_2 or 18 mM NaOH for 0, 2, or 4 h. p—SREBP2 precursor (approximately 126 kD); c—SREBP2 cleaved form (approximately 68 kD); (pooled sample of $n = 3$ biological replicates). **(B)** Quantitative PCR analysis for the expression levels of CO_2 responsive genes from control (siNTC) or SREBP2 silenced (siSREBP2) NIH3T3 cells exposed to 5% or 1% CO_2 for 4 h (mean ± SE, $n = 3$ biological replicates per condition, $^{***}P < 0.001$, $^{**}P < 0.01$, nonsignificant (ns), two-way ANOVA with Bonferroni's multiple comparisons test). The data underlying the graphs shown in the figure is included in S1 Data.
(TIF)

S5 Fig. CO_2 levels modulate the response of an SRE bioluminescence reporter. (A) Bioluminescence recordings from NIH3T3 cells transfected with WT SRE-Luc, or control vector

(CMV-Luc), and exposed to either 5%, 1%, or 10% CO_2, arrow indicates the shift in CO_2 levels (mean ± SE, $n = 3$ biological replicate per condition, AUC for SRE Luc 5%, 1% CO_2 0.77 ± 0.01, 2.6 ± 0.1, $P < 0.0001$ and 5%, 10% CO_2 1.04 ± 0.005, 0.65 ± 0.02, $P < 0.0001$; AUC for CMV Luc 5%, 1% CO_2 0.2 ± 0.002, 0.19 ± 0.005, ns and 5%, 10% CO_2 0.65 ± 0.02, 0.68 ± 0.01, ns, nonsignificant (ns), two-sided Student's *t* test). **(B)** Bioluminescence recordings from NIH3T3 cells transfected with WT SRE-Luc exposed either to constant 5% or interchangeable 5% to 1% CO_2 levels, blue mark represents 5%, and red mark indicates 1% CO_2 levels (mean ± SE, $n = 3$ biological replicate per condition). The data underlying the graphs shown in the figure is included in S1 Data.
(TIF)

S6 Fig. Systematic dissection of SREBP2 pathway activation in response to low CO_2 levels. **(A)** Schematic representation of the SREBP2 pathway, specifying interventions applied at different stages in the following experiments. **(B, C)** Immunoblots of total cell lysates from NIH3T3 cells either non-transfected or transfected with 2X-FLAG tagged N-SREBP2. Cells were either sterol-depleted with methyl-beta-cyclodextrin (MBCD) or CO_2 treated for 4 h (pooled sample from $n = 3$ biological replicates). **(D)** Immunoblot of total cell lysates from NIH3T3 cells exposed to different CO_2 levels in presence of DMSO or fatostatin (20 μm) for 4 h (pooled sample from $n = 3$ biological replicates). **(E)** Quantitative PCR analysis of cholestrogenic gene expression levels from cells as in (D), (mean ± SE, $n = 3$ biological replicates for each time point per condition, $^{***}P < 0.001$, nonsignificant (ns), two-way ANOVA with Bonferroni's multiple comparisons test). **(F)** Quantitative PCR analysis of cholestrogenic gene expression levels from NIH3T3 cells silenced for SCAP (siSCAP) or control siRNA (siNTC) upon exposure to either 5% or 1% CO_2 levels for 4 h (mean ± SE, $n = 3$ biological replicates for each time point per condition, $^{***}P < 0.001$, nonsignificant (ns), two-way ANOVA with Bonferroni's multiple comparisons test). The data underlying the graphs shown in the figure is included in S1 Data.
(TIF)

S7 Fig. Exposure to low CO_2 levels decreases ER cholesterol levels. **(A)** Total cholesterol quantification (with fluorometric assay kit) in NIH3T3 cells exposed to 10% CO_2 levels for 4 h (mean ± SE, $n = 3$ biological replicates per condition, nonsignificant (ns), two-sided Student's *t* test). **(B)** Flow chart representing the different steps taken for ER-membrane isolation by sucrose gradient. **(C)** Immunoblot analysis of organelle protein markers in each fraction throughout the isolation process (as detailed in panel B). **(D)** The free cholesterol and cholesterol ester levels in the ER membrane from NIH3T3 cells depleted with sterols for 2 h or exposed to different CO_2 levels for 4 h were quantified with shotgun lipidomics analysis (see S5 Table) (mean ± SE, $n = 3$ independent experiments, two-sided Student's *t* test). The data is from Fig 4C and 4D corrected to ER protein amounts. The data underlying the graphs shown in the figure is included in S1 Data.
(TIF)

S1 Table. Transcriptional response to low CO_2 and NaOH (separate file). List of differentially expressed genes from NIH3T3 cells treated with either low CO_2 or 18 mM NaOH for 2 h and 4 h.
(XLSX)

S2 Table. K-Mean cluster analysis (separate file). List of genes that were categorized the clusters for described in Fig 2 for NIH3T3 cells treated with either low CO_2 or 18 mM NaOH for 2 h and 4 h.
(XLSX)

S3 Table. Pathway enrichment analysis (separate file). Full list of processes enriched in different clusters (as in Fig 2A) in NIH3T3 cells exposed to 5%, 1% CO_2 or treated with 18 mM NaOH for 2 h and 4 h.
(XLSX)

S4 Table. Upstream gene expression regulator analysis (separate file). Full list of upstream gene expression regulators in the different clusters (as in Fig 3A and 3B) in NIH3T3 cells exposed to either low CO_2 or NaOH for 2 h and 4 h.
(XLSX)

S5 Table. ER lipidomics analysis (separate file). Measurement of cholesterol and cholesterol ester different classes of ER lipids with shot gun lipidomics in ER fractions isolated from NIH3T3 cells either depleted for sterols for exposed to 5% CO_2 or 1% CO_2 for 4 h.
(XLSX)

S6 Table. Chemicals and reagents (separate file). List of reagents and chemicals that were used in the study including their manufactures and catalogue numbers.
(XLSX)

S7 Table. List of primers used for quantitative real-time PCR (separate file). Primers used for quantitative PCR analysis are listed in the table.
(XLSX)

S8 Table. List of antibodies (separate file). Antibodies and the dilutions used for immunoblot analysis are detailed in the table.
(XLSX)

S1 Data. Original data for the different graphs (separate file). Each tab includes data for individual panels of main and supplementary figures as referred to in the figure captions.
(XLSX)

S1 Raw Images. Original blots (separate file). The file contains the original and unprocessed blots that are presented in main and supplementary figures.
(PPTX)

Acknowledgments

We are grateful to all the members of the Asher lab for their comments on the manuscript. We also would like acknowledge Moshe Goldsmith for the helpful discussion on carbonic anhydrase biochemistry. Graphical illustrations were generated with BioRender.com.

Author Contributions

Conceptualization: Nityanand Bolshette, Gad Asher.

Investigation: Nityanand Bolshette, Saar Ezagouri, Vaishnavi Dandavate, Iuliia Karavaeva, Marina Golik, Hu Wang, Xianlin Han.

Resources: Peter J. Espenshade, Timothy F. Osborne.

Supervision: Gad Asher.

Writing – original draft: Nityanand Bolshette, Gad Asher.

References

1. Schofield CJ, Ratcliffe PJ. Oxygen sensing by HIF hydroxylases. Nat Rev Mol Cell Biol. 2004; 5 (5):343–354. Epub 2004/05/04. https://doi.org/10.1038/nrm1366 PMID: 15122348.
2. Kim JW, Tchernyshyov I, Semenza GL, Dang CV. HIF-1-mediated expression of pyruvate dehydrogenase kinase: a metabolic switch required for cellular adaptation to hypoxia. Cell Metab. 2006; 3(3):177–185. Epub 2006/03/07. https://doi.org/10.1016/j.cmet.2006.02.002 PMID: 16517405.
3. Semenza GL. Hypoxia-inducible factors in physiology and medicine. Cell. 2012; 148(3):399–408. Epub 2012/02/07. https://doi.org/10.1016/j.cell.2012.01.021 PMID: 22304911; PubMed Central PMCID: PMC3437543.
4. Patel S, Miao JH, Yetiskul E, Anokhin A, Majmundar SH. Physiology, Carbon Dioxide Retention. StatPearls. Treasure Island (FL). 2022.
5. Shigemura M, Lecuona E, Angulo M, Homma T, Rodriguez DA, Gonzalez-Gonzalez FJ, et al. Hypercapnia increases airway smooth muscle contractility via caspase-7-mediated miR-133a-RhoA signaling. Sci Transl Med. 2018; 10(457). Epub 2018/09/07. https://doi.org/10.1126/scitranslmed.aat1662 PMID: 30185650; PubMed Central PMCID: PMC6889079.
6. Bharat A, Angulo M, Sun H, Akbarpour M, Alberro A, Cheng Y, et al. High CO(2) Levels Impair Lung Wound Healing. Am J Respir Cell Mol Biol. 2020; 63(2):244–254. Epub 2020/04/11. https://doi.org/10.1165/rcmb.2019-0354OC PMID: 32275835; PubMed Central PMCID: PMC7397765.
7. O'Toole D, Hassett P, Contreras M, Higgins BD, McKeown ST, McAuley DF, et al. Hypercapnic acidosis attenuates pulmonary epithelial wound repair by an NF-kappaB dependent mechanism. Thorax. 2009; 64(11):976–982. Epub 2009/07/21. https://doi.org/10.1136/thx.2008.110304 PMID: 19617214.
8. Hopkins E, Sanvictores T, Sharma S. Physiology, Acid Base Balance. StatPearls. Treasure Island (FL). 2023.
9. Adamovich Y, Ladeuix B, Golik M, Koeners MP, Asher G. Rhythmic Oxygen Levels Reset Circadian Clocks through HIF1alpha. Cell Metab. 2017; 25(1):93–101. Epub 2016/10/25. https://doi.org/10.1016/j.cmet.2016.09.014 PMID: 27773695.
10. Phelan DE, Mota C, Strowitzki MJ, Shigemura M, Sznajder JI, Crowe L, et al. Hypercapnia alters mitochondrial gene expression and acylcarnitine production in monocytes. Immunol Cell Biol. 2023; 101 (6):556–577. Epub 2023/03/28. https://doi.org/10.1111/imcb.12642 PMID: 36967673; PubMed Central PMCID: PMC10330468.
11. Brown MS, Goldstein JL. The SREBP pathway: regulation of cholesterol metabolism by proteolysis of a membrane-bound transcription factor. Cell. 1997; 89(3):331–340. Epub 1997/05/02. https://doi.org/10.1016/s0092-8674(00)80213-5 PMID: 9150132.
12. Horton JD, Goldstein JL, Brown MS. SREBPs: activators of the complete program of cholesterol and fatty acid synthesis in the liver. J Clin Invest. 2002; 109(9):1125–1131. Epub 2002/05/08. https://doi.org/10.1172/JCI15593 PMID: 11994399; PubMed Central PMCID: PMC150968.
13. Sakai J, Duncan EA, Rawson RB, Hua X, Brown MS, Goldstein JL. Sterol-regulated release of SREBP-2 from cell membranes requires two sequential cleavages, one within a transmembrane segment. Cell. 1996; 85(7):1037–1046. Epub 1996/06/28. https://doi.org/10.1016/s0092-8674(00)81304-5 PMID: 8674110.
14. Ye J, DeBose-Boyd RA. Regulation of cholesterol and fatty acid synthesis. Cold Spring Harb Perspect Biol. 2011; 3(7). Epub 2011/04/21. https://doi.org/10.1101/cshperspect.a004754 PMID: 21504873; PubMed Central PMCID: PMC3119913.
15. Dooley KA, Millinder S, Osborne TF. Sterol regulation of 3-hydroxy-3-methylglutaryl-coenzyme A synthase gene through a direct interaction between sterol regulatory element binding protein and the trimeric CCAAT-binding factor/nuclear factor Y. J Biol Chem. 1998; 273(3):1349–1356. Epub 1998/01/27. https://doi.org/10.1074/jbc.273.3.1349 PMID: 9430668.
16. Roglans N, Verd JC, Peris C, Alegret M, Vazquez M, Adzet T, et al. High doses of atorvastatin and simvastatin induce key enzymes involved in VLDL production. Lipids. 2002; 37(5):445–454. Epub 2002/06/12. https://doi.org/10.1007/s11745-002-0916-0 PMID: 12056585.
17. Kamisuki S, Mao Q, Abu-Elheiga L, Gu Z, Kugimiya A, Kwon Y, et al. A small molecule that blocks fat synthesis by inhibiting the activation of SREBP. Chem Biol. 2009; 16(8):882–892. Epub 2009/09/01. https://doi.org/10.1016/j.chembiol.2009.07.007 PMID: 19716478.
18. Smith JR, Osborne TF, Brown MS, Goldstein JL, Gil G. Multiple sterol regulatory elements in promoter for hamster 3-hydroxy-3-methylglutaryl-coenzyme A synthase. J Biol Chem. 1988; 263(34):18480–18487. Epub 1988/12/05. PMID: 2903862.
19. Viviani VR, Arnoldi FG, Neto AJ, Oehlmeyer TL, Bechara EJ, Ohmiya Y. The structural origin and biological function of pH-sensitivity in firefly luciferases. Photochem Photobiol Sci. 2008; 7(2):159–169. Epub 2008/02/12. https://doi.org/10.1039/b714392c PMID: 18264583.

20. Yang T, Espenshade PJ, Wright ME, Yabe D, Gong Y, Aebersold R, et al. Crucial step in cholesterol homeostasis: sterols promote binding of SCAP to INSIG-1, a membrane protein that facilitates retention of SREBPs in ER. Cell. 2002; 110(4):489–500. Epub 2002/08/31. https://doi.org/10.1016/s0092-8674(02)00872-3 PMID: 12202038.

21. Luo J, Yang H, Song BL. Mechanisms and regulation of cholesterol homeostasis. Nat Rev Mol Cell Biol. 2020; 21(4):225–245. Epub 2019/12/19. https://doi.org/10.1038/s41580-019-0190-7 PMID: 31848472.

22. Wang X, Sato R, Brown MS, Hua X, Goldstein JL. SREBP-1, a membrane-bound transcription factor released by sterol-regulated proteolysis. Cell. 1994; 77(1):53–62. Epub 1994/04/08. https://doi.org/10.1016/0092-8674(94)90234-8 PMID: 8156598.

23. Hirano Y, Yoshida M, Shimizu M, Sato R. Direct demonstration of rapid degradation of nuclear sterol regulatory element-binding proteins by the ubiquitin-proteasome pathway. J Biol Chem. 2001; 276(39):36431–36437. Epub 2001/07/31. https://doi.org/10.1074/jbc.M105200200 PMID: 11477106.

24. Sundqvist A, Bengoechea-Alonso MT, Ye X, Lukiyanchuk V, Jin J, Harper JW, et al. Control of lipid metabolism by phosphorylation-dependent degradation of the SREBP family of transcription factors by SCF(Fbw7). Cell Metab. 2005; 1(6):379–391. Epub 2005/08/02. https://doi.org/10.1016/j.cmet.2005.04.010 PMID: 16054087.

25. Toth JI, Datta S, Athanikar JN, Freedman LP, Osborne TF. Selective coactivator interactions in gene activation by SREBP-1a and -1c. Mol Cell Biol. 2004; 24(18):8288–8300. Epub 2004/09/02. https://doi.org/10.1128/MCB.24.18.8288-8300.2004 PMID: 15340088; PubMed Central PMCID: PMC515064.

26. Esquejo RM, Roqueta-Rivera M, Shao W, Phelan PE, Seneviratne U, Am Ende CW, et al. Dipyridamole Inhibits Lipogenic Gene Expression by Retaining SCAP-SREBP in the Endoplasmic Reticulum. Cell Chem Biol. 2021; 28(2):169–179 e7. Epub 2020/10/24. https://doi.org/10.1016/j.chembiol.2020.10.003 PMID: 33096051; PubMed Central PMCID: PMC7897222.

27. Gao Y, Zhou Y, Goldstein JL, Brown MS, Radhakrishnan A. Cholesterol-induced conformational changes in the sterol-sensing domain of the Scap protein suggest feedback mechanism to control cholesterol synthesis. J Biol Chem. 2017; 292(21):8729–8737. Epub 2017/04/06. https://doi.org/10.1074/jbc.M117.783894 PMID: 28377508; PubMed Central PMCID: PMC5448100.

28. Rawson RB, DeBose-Boyd R, Goldstein JL, Brown MS. Failure to cleave sterol regulatory element-binding proteins (SREBPs) causes cholesterol auxotrophy in Chinese hamster ovary cells with genetic absence of SREBP cleavage-activating protein. J Biol Chem. 1999; 274(40):28549–28556. Epub 1999/09/25. https://doi.org/10.1074/jbc.274.40.28549 PMID: 10497220.

29. Lee SH, Lee JH, Im SS. The cellular function of SCAP in metabolic signaling. Exp Mol Med. 2020; 52(5):724–729. Epub 2020/05/10. https://doi.org/10.1038/s12276-020-0430-0 PMID: 32385422; PubMed Central PMCID: PMC7272406.

30. Radhakrishnan A, Goldstein JL, McDonald JG, Brown MS. Switch-like control of SREBP-2 transport triggered by small changes in ER cholesterol: a delicate balance. Cell Metab. 2008; 8(6):512–521. Epub 2008/12/02. https://doi.org/10.1016/j.cmet.2008.10.008 PMID: 19041766; PubMed Central PMCID: PMC2652870.

31. Infante RE, Radhakrishnan A. Continuous transport of a small fraction of plasma membrane cholesterol to endoplasmic reticulum regulates total cellular cholesterol. Elife. 2017; 6. Epub 2017/04/18. https://doi.org/10.7554/eLife.25466 PMID: 28414269; PubMed Central PMCID: PMC5433840.

32. Lange Y, Ye J, Rigney M, Steck TL. Regulation of endoplasmic reticulum cholesterol by plasma membrane cholesterol. J Lipid Res. 1999; 40(12):2264–2270. Epub 1999/12/10. PMID: 10588952.

33. Robba C, Siwicka-Gieroba D, Sikter A, Battaglini D, Dabrowski W, Schultz MJ, et al. Pathophysiology and clinical consequences of arterial blood gases and pH after cardiac arrest. Intensive Care Med Exp. 2020; 8(Suppl 1):19. Epub 2020/12/19. https://doi.org/10.1186/s40635-020-00307-1 PMID: 33336311; PubMed Central PMCID: PMC7746422.

34. Vohwinkel CU, Lecuona E, Sun H, Sommer N, Vadasz I, Chandel NS, et al. Elevated CO(2) levels cause mitochondrial dysfunction and impair cell proliferation. J Biol Chem. 2011; 286(43):37067–37076. Epub 2011/09/10. https://doi.org/10.1074/jbc.M111.290056 PMID: 21903582; PubMed Central PMCID: PMC3199454.

35. Launois S, Clergue F, Medrano G, Similowski T, Aubier M, Murciano D, et al. The control of respiration in pulmonary fibrosis. The effect of O2 and CO2. Rev Mal Respir. 1991; 8(1):67–73. Epub 1991/01/01. PMID: 1903551.

36. Zhao J, Hogan EM, Bevensee MO, Boron WF. Out-of-equilibrium CO2/HCO3- solutions and their use in characterizing a new K/HCO3 cotransporter. Nature. 1995; 374(6523):636–639. Epub 1995/04/13. https://doi.org/10.1038/374636a0 PMID: 7715702.

37. Kondo A, Yamamoto S, Nakaki R, Shimamura T, Hamakubo T, Sakai J, et al. Extracellular Acidic pH Activates the Sterol Regulatory Element-Binding Protein 2 to Promote Tumor Progression. Cell Rep.

2017; 18(9):2228–2242. Epub 2017/03/02. https://doi.org/10.1016/j.celrep.2017.02.006 PMID: 28249167.

38. Cummins EP, Selfridge AC, Sporn PH, Sznajder JI, Taylor CT. Carbon dioxide-sensing in organisms and its implications for human disease. Cell Mol Life Sci. 2014; 71(5):831–845. Epub 2013/09/21. https://doi.org/10.1007/s00018-013-1470-6 PMID: 24045706; PubMed Central PMCID: PMC3945669.

39. Casalino-Matsuda SM, Wang N, Ruhoff PT, Matsuda H, Nlend MC, Nair A, et al. Hypercapnia Alters Expression of Immune Response, Nucleosome Assembly and Lipid Metabolism Genes in Differentiated Human Bronchial Epithelial Cells. Sci Rep. 2018; 8(1):13508. Epub 2018/09/12. https://doi.org/10.1038/s41598-018-32008-x PMID: 30202079; PubMed Central PMCID: PMC6131151.

40. Adamovich Y, Ladeuix B, Sobel J, Manella G, Neufeld-Cohen A, Assadi MH, et al. Oxygen and Carbon Dioxide Rhythms Are Circadian Clock Controlled and Differentially Directed by Behavioral Signals. Cell Metab. 2019; 29(5):1092–1103 e3. Epub 2019/02/19. https://doi.org/10.1016/j.cmet.2019.01.007 PMID: 30773466.

41. Parathath S, Mick SL, Feig JE, Joaquin V, Grauer L, Habiel DM, et al. Hypoxia is present in murine atherosclerotic plaques and has multiple adverse effects on macrophage lipid metabolism. Circ Res. 2011; 109(10):1141–1152. Epub 2011/09/17. https://doi.org/10.1161/CIRCRESAHA.111.246363 PMID: 21921268; PubMed Central PMCID: PMC3208906.

42. Vaidyanathan S, Salmi TM, Sathiqu RM, McConville MJ, Cox AG, Brown KK. YAP regulates an SGK1/mTORC1/SREBP-dependent lipogenic program to support proliferation and tissue growth. Dev Cell. 2022; 57(6):719–731 e8. Epub 2022/02/27. https://doi.org/10.1016/j.devcel.2022.02.004 PMID: 35216681.

43. Shu Z, Gao Y, Zhang G, Zhou Y, Cao J, Wan D, et al. A functional interaction between Hippo-YAP signalling and SREBPs mediates hepatic steatosis in diabetic mice. J Cell Mol Med. 2019; 23(5):3616–3628. Epub 2019/03/02. https://doi.org/10.1111/jcmm.14262 PMID: 30821074; PubMed Central PMCID: PMC6484311.

44. Itel F, Al-Samir S, Oberg F, Chami M, Kumar M, Supuran CT, et al. CO2 permeability of cell membranes is regulated by membrane cholesterol and protein gas channels. FASEB J. 2012; 26(12):5182–5191. Epub 2012/09/12. https://doi.org/10.1096/fj.12-209916 PMID: 22964306.

45. Arias-Hidalgo M, Al-Samir S, Gros G, Endeward V. Cholesterol is the main regulator of the carbon dioxide permeability of biological membranes. Am J Physiol Cell Physiol. 2018; 315(2):C137–C140. Epub 2018/06/07. https://doi.org/10.1152/ajpcell.00139.2018 PMID: 29874108.

46. Mullen PJ, Yu R, Longo J, Archer MC, Penn LZ. The interplay between cell signalling and the mevalonate pathway in cancer. Nat Rev Cancer. 2016; 16(11):718–731. Epub 2016/10/25. https://doi.org/10.1038/nrc.2016.76 PMID: 27562463.

47. Aviram R, Dandavate V, Manella G, Golik M, Asher G. Ultradian rhythms of AKT phosphorylation and gene expression emerge in the absence of the circadian clock components Per1 and Per2. PLoS Biol. 2021; 19(12):e3001492. Epub 2021/12/31. https://doi.org/10.1371/journal.pbio.3001492 PMID: 34968386; PubMed Central PMCID: PMC8718012.

48. Eigler T, Zarfati G, Amzallag E, Sinha S, Segev N, Zabary Y, et al. ERK1/2 inhibition promotes robust myotube growth via CaMKII activation resulting in myoblast-to-myotube fusion. Dev Cell. 2021; 56(24):3349–3363e6. Epub 2021/12/22. https://doi.org/10.1016/j.devcel.2021.11.022 PMID: 34932950; PubMed Central PMCID: PMC8693863.

49. Sustarsic EG, Ma T, Lynes MD, Larsen M, Karavaeva I, Havelund JF, et al. Cardiolipin Synthesis in Brown and Beige Fat Mitochondria Is Essential for Systemic Energy Homeostasis. Cell Metab. 2018; 28(1):159–174 e11. Epub 2018/06/05. https://doi.org/10.1016/j.cmet.2018.05.003 PMID: 29861389; PubMed Central PMCID: PMC6038052.

50. Jaitin DA, Kenigsberg E, Keren-Shaul H, Elefant N, Paul F, Zaretsky I, et al. Massively parallel single-cell RNA-seq for marker-free decomposition of tissues into cell types. Science. 2014; 343(6172):776–779. Epub 2014/02/18. https://doi.org/10.1126/science.1247651 PMID: 24531970; PubMed Central PMCID: PMC4412462.

51. Kohen R, Barlev J, Hornung G, Stelzer G, Feldmesser E, Kogan K, et al. UTAP: User-friendly Transcriptome Analysis Pipeline. BMC Bioinformatics. 2019; 20(1):154. Epub 2019/03/27. https://doi.org/10.1186/s12859-019-2728-2 PMID: 30909881; PubMed Central PMCID: PMC6434621.

52. Anders S, Pyl PT, Huber W. HTSeq—a Python framework to work with high-throughput sequencing data. Bioinformatics. 2015; 31(2):166–169. Epub 2014/09/28. https://doi.org/10.1093/bioinformatics/btu638 PMID: 25260700; PubMed Central PMCID: PMC4287950.

53. Dobin A, Davis CA, Schlesinger F, Drenkow J, Zaleski C, Jha S, et al. STAR: ultrafast universal RNA-seq aligner. Bioinformatics. 2013; 29(1):15–21. Epub 2012/10/30. https://doi.org/10.1093/bioinformatics/bts635 PMID: 23104886; PubMed Central PMCID: PMC3530905.

54. Love MI, Huber W, Anders S. Moderated estimation of fold change and dispersion for RNA-seq data with DESeq2. Genome Biol. 2014; 15(12):550. Epub 2014/12/18. https://doi.org/10.1186/s13059-014-0550-8 PMID: 25516281; PubMed Central PMCID: PMC4302049.

55. Han X. Lipidomics: Comprehensive Mass Spectrometry of Lipids/Xianlin Han. United States of Ameria, John Wiley & Sons, Inc., Hoboken, New Jersey; 2016.

56. Wang M, Han X. Multidimensional mass spectrometry-based shotgun lipidomics. Methods Mol Biol. 2014; 1198:203–220. https://doi.org/10.1007/978-1-4939-1258-2_13 PMID: 25270931; PubMed Central PMCID: PMC4261229.

57. Han X, Yang K, Gross RW. Microfluidics-based electrospray ionization enhances the intrasource separation of lipid classes and extends identification of individual molecular species through multi-dimensional mass spectrometry: development of an automated high-throughput platform for shotgun lipidomics. Rapid Commun Mass Spectrom. 2008; 22(13):2115–2124. https://doi.org/10.1002/rcm.3595 PMID: 18523984; PubMed Central PMCID: PMC2927983.

58. Wang M, Wang C, Han RH, Han X. Novel advances in shotgun lipidomics for biology and medicine. Prog Lipid Res. 2016; 61:83–108. https://doi.org/10.1016/j.plipres.2015.12.002 PMID: 26703190; PubMed Central PMCID: PMC4733395.

59. Yang K, Cheng H, Gross RW, Han X. Automated lipid identification and quantification by multidimensional mass spectrometry-based shotgun lipidomics. Anal Chem. 2009; 81(11):4356–4368. https://doi.org/10.1021/ac900241u PMID: 19408941; PubMed Central PMCID: PMC2728582.